Tilted Janus Polymer Pillars

Myoung-Woon Moon, Tae-Gon Cha,

Kwang-Ryeol Lee, Ashkan Vaziri, and Ho-Young Kim

Supplementary Materials

Appendix 1: Shrinkage strain induced by low energy focused ion beam

To quantify the shrinkage of the polymer surface due to ion beam irradiation, we designed an additional set of experiment, where micropillars are subjected to ion beam with incident angle of 0^o (parallel to the micropillars directions and normal to the polymer surface), Fig. S1A. The top surface of the micropillars shrinks almost uniformly due the ion beam irradiation as shown in Fig. S1B. The shrinkage strain can be estimated using $\varepsilon = (R_1 - R_0)/R_0$, where R_0 is the radius of micropillars prior to exposure to FIB and R_1 is the radius of the top of micropillars after ion beam irradiation, as denoted in Fig. S1C.

The underlying mechanisms of this phenomenon is ambiguous, however, it is conceivable that thermal stresses results in this shrinkage. Ion beam irradiation results in high temperature at the surface, which after cooling down to the room temperature could lead to significant shrinkage of the stiff skin induced on the surface of the polymer. The induced strain in the stiff skin can be estimated by measuring the reduction in the pillar diameter at the top of the micropillars and is quantified in Fig. 2B for various treatment durations.

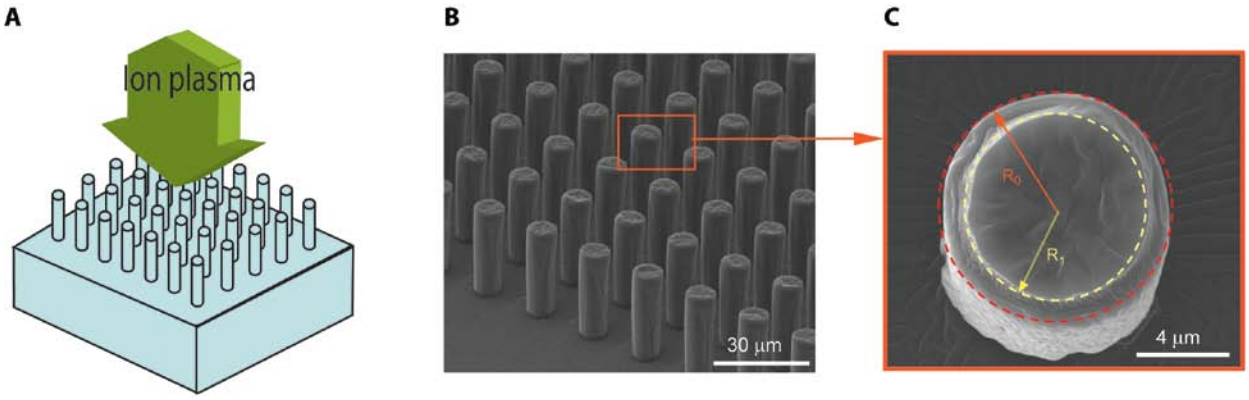

Fig. S1 Measuring the shrinkage strain induced by ion beam irradiation. (A) Schematic of the experiment. (B) SEM image of the micropillars exposed to ion beam with incident angle of 0^o. (C) SEM image of single micropillars after FIB irradiation. The micropillars have original diameter of 9.45 μm, which is reduced at the top layer to 7.77 μm after 20 min ion beam irradiation.

Appendix 2: Contact behavior of tilted and straight micropillars.

We acquired the optical images of straight and titled micropillar arrays as they are indented by a spherical steel ball. On straight micropillar arrays, each pillar may experience buckling along axial direction and the contacting area remains circular as the indentation displacement increases. For tilted pillar arrays, the tilted micropillars undergo bending and the contact area increases. A yellow arrow indicate the tilting direction of each pillar.

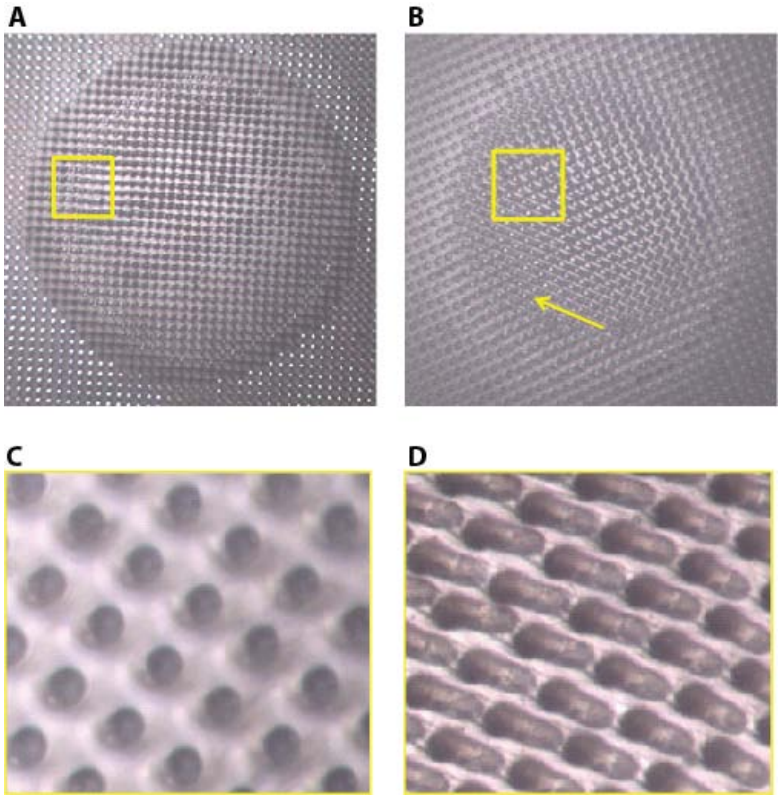

Fig. S2. Optical images for straight (A, C) and tilted (B, D) micropillars under loading condition. For the straight micropillar array, the image was taken at the preload ~ 8mN and indention depth ~ 23 μm. For the tiled micropillar array, the image was taken at the same preload, which correspond to the indenting depth ~ 20 μm. C and D are magnified images from yellow boxes in A and B, respectively.

Appendix 3: Sliding speed dependency of coefficient of friction

To explore the dependence of the friction behavior of tilted pillars on the sliding speed, we carried out a friction test over a wide range of sliding speeds (2 - 50 μm/sec) against a glass ball with 4 cm in diameter. Our results are summarized in Fig. S3 for sliding on titled

micropillars in against and along tilting directions. Our results show that the COF for sliding along the tilting direction of micropillars minimally depends on the sliding speed, which is consistent with the result from a literature. In contrast, the COF for sliding against the micropillar tilting direction increased remarkably by increasing the sliding speed.

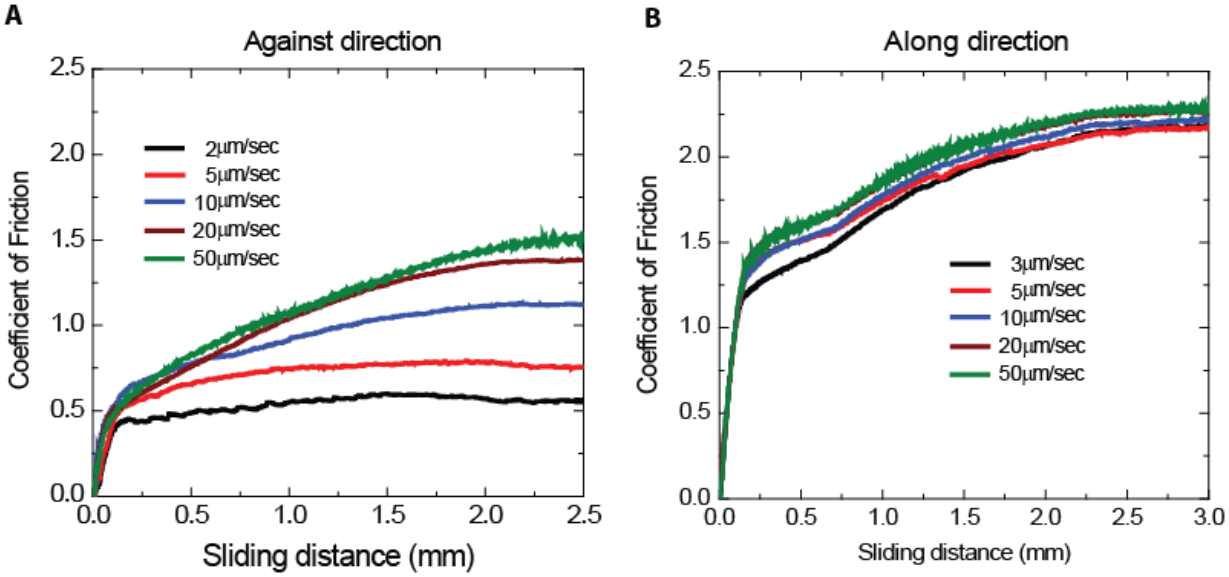

Fig. S3. Coefficient of friction versus the sliding distance for sliding in two different directions. In this set of experiments, the normal force (denoted as pre-load in Fig. 4D) was 400 mN. The micropillars had the titling angle of 32^{o} and have the same dimensions as Fig. 4E.